A Practical Approach to Produce Mg-Al Spinel Based on the Modeling of Phase Equilibria for NH_4Cl-$MgCl_2$-$AlCl_3$-H_2O System

Wencheng Gao and Zhibao Li

Key Laboratory of Green Process and Engineering, National Engineering Laboratory for Hydrometallurgical Cleaner Production Technology, Institute of Process Engineering, Chinese Academy of Sciences, Beijing 100190, P. R. China

DOI 10.1002/aic.13963

Published online November 30, 2012 in Wiley Online Library (wileyonlinelibrary.com).

Based on chemical modeling of phase equilibria for the NH_4Cl-$MgCl_2$-$AlCl_3$-H_2O system, a practical approach to produce Mg-Al spinel ($MgAl_2O_4$) (widely used as refractory brick, supports in catalysts, and inert material for oxygen carriers) is proposed and proven feasible. This novel process includes coprecipitation of $Mg_4Al_2(OH)_{14}\cdot 3H_2O$ from the NH_3-$MgCl_2$-$AlCl_3$-H_2O system; calcination of $Mg_4Al_2(OH)_{14}\cdot 3H_2O$ to obtain Mg-Al spinel and recovery of NH_4Cl from NH_4Cl-rich solutions by feeding $MgCl_2$-$AlCl_3$. A MSMPR reactor was applied to investigate the effect of temperature, feed concentration, and NH_4Cl addition on coprecipitation of precursor $Mg_4Al_2(OH)_{14}\cdot 3H_2O$ from $MgCl_2$-$AlCl_3$ solutions with Mg/Al ratio 2 through gradual addition of NH_4OH. The phase equilibria of the NH_4Cl-$MgCl_2$-$AlCl_3$-H_2O system were determined over the temperature range 283.2 to 363.2 K using dynamic method. The experimental solubilities were regressed to obtain new Bromley-Zemaitis model parameters. These newly obtained parameters were verified by predicting the quaternary system. A chemical model for the NH_4Cl-$MgCl_2$-$AlCl_3$-H_2O system has been established with the OLI platform. All the results generated from this study will provide the theoretical basis for Mg-Al spinel production. The high quality Mg-Al spinel was prepared by calcination of precursor from 773.2 to 1273.2 K, and the NH_4Cl was successfully recovered through the common ion effect of $MgCl_2$-$AlCl_3$ addition. *AIChE J,* 59: 1855–1867, 2013

Keywords: Mg-Al spinel, coprecipitation, solubility, phase equilibria, chemical modeling

Introduction

Low-grade aluminum resources, such as kaolinitic clay,[1] fly ash,[2] and diaspore,[3] are rich in their reserve around the world. Much research has been performed to extract aluminum from these resources. There are mainly two methods frequently applied to achieve this goal: alkali leaching[4–7] and acid leaching.[4,5,8–10] In the process of alkali leaching, the alkali concentration is a significant factor in controlling the leaching of aluminum. Higher alkali concentration leads to much higher silica dissolved in NaOH-$NaAl(OH)_4$ solutions due to the low ratios of alumina to silica (Al/Si $\leq$ 1) in these low grade resources. Extensive research has thus been conducted to develop a process to prepare alumina through acid leaching.[11,12] For example, the U.S. Bureau of Mines conducted a series of studies to recover alumina by the calcination of $AlCl_3\cdot 6H_2O$ obtained from HCl acid leaching of clay.[13–18] In their process, calcined clay is leached with 26–36% HCl and $AlCl_3\cdot 6H_2O$ was crystallized from the purified pregnant liquor by injecting HCl gas. However, there is a big challenge to deal with the environmental problem caused by concentrated HCl use in the step of $AlCl_3\cdot 6H_2O$ crystallization. As alternative, it may be possible to use $AlCl_3$ solution directly to prepare high-quality Mg-Al spinel by coprecipitation with $MgCl_2$ brines generated in large abundance as by-product or waste in the potassium fertilizer industry.[19]

Mg-Al spinel has been applied widely to make a variety of refractories as it offers a good combination of physical and chemical properties such as excellent thermal shock resistance and high chemical inertness.[20] It has also been used as a catalyst support and as porous support (inert material) for oxygen carriers such as NiO, Fe_2O_3, CuO, and so on in chemical-looping combustion.[21–23] Among its synthesis methods, coprecipitation[24,25] has attracted attention because of relative convenience and cost-effectiveness. In our laboratory, a new process to produce Mg-Al spinel through coprecipitation of magnesium and aluminum from $MgCl_2$-$AlCl_3$ solution is under development. The preliminary study was carried out from diluted $MgCl_2$-$AlCl_3$ solutions in a batch system[26] by the following reaction (1):

$$4MgCl_2 + 2AlCl_3 + 14NH_4OH + 3H_2O \rightarrow Mg_4Al_2(OH)_{14}\cdot 3H_2O(s) + 14NH_4Cl \quad (1)$$

In previous work,[26] the K_{SP} and thermodynamic properties of $Mg_4Al_2(OH)_{14}\cdot 3H_2O$ were determined, and the precipitation diagram of Mg-Al-OH was constructed. However, it was impossible to scale up such a batch precipitation

Correspondence concerning this article should be addressed to Z. Li at zhibaoli@home.ipe.ac.cn.

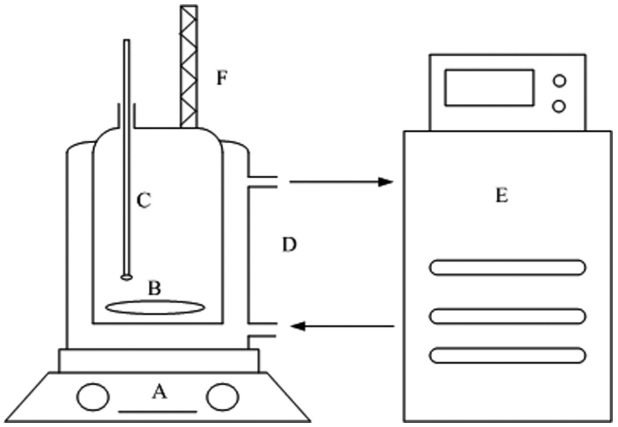

Figure 1. Experimental equipment.

A, magnetic stirring apparatus; B, magnetic rotor; C, thermometer; D, vessel; E, band heater; F, condenser.

process for industrial application due to two main problems: (1) the synthesized $Mg_4Al_2(OH)_{14}\cdot 3H_2O$ was difficult to filter from the highly dispersed colloidal solution; (2) the generated NH_4Cl with very low concentration (<0.5 mol L^{-1}) could not be effectively recovered by currently existing methods.

To tackle these problems, in this work a mixed-suspension mixed-product removal (MSMPR) reactor was applied to produce $Mg_4Al_2(OH)_{14}\cdot 3H_2O$ with excellent filterability and to generate concentrated NH_4Cl solution. The obtained NH_4Cl-rich solutions provided an opportunity to recover NH_4Cl with the aid of the common ion effect[27] by feeding $MgCl_2$-$AlCl_3$ (Mg/Al = 2). Therefore, it is necessary to study on the phase equilibria of the NH_4Cl-$MgCl_2$-$AlCl_3$-H_2O system. Limited solubility data for this system have been reported in the literature. Wang and Li[19] determined the solid–liquid equilibria of the ternary NH_4Cl-$MgCl_2$-H_2O system at temperatures from 278.15 to 348.15 K. Christov[28] only measured the solubility of the $MgCl_2$-$AlCl_3$-H_2O system at 298.15 K. Much more phase equilibria are required to accomplish the development, design, and simulation of this novel NH_4Cl recovery process for the production of $Mg_4Al_2(OH)_{14}\cdot 3H_2O$.

In this article, the determination and chemical modeling of phase equilibria for the NH_4Cl-$MgCl_2$-$AlCl_3$-H_2O system were performed from 283.2–363.2 K. The Bromley-Zemaitis model was used to regress new parameters of ion–ion interactions. Then, the effect of parameters on coprecipitation, including temperature, feed concentration, and NH_4Cl addition was investigated in a MSMPR reactor. Furthermore, the Mg-Al spinel was produced by calcination of $Mg_4Al_2(OH)_{14}\cdot 3H_2O$ at 773.2–1273.2 K. Finally, a new practical approach to produce Mg-Al spinel was proposed and verified feasible based on the modeling and precipitation tests. All the results generated from this study will provide the fundamentals for future industrial scale up for this new process.

Experimental Procedure

Chemical agents

Ammonium chloride (99.5%, Xilong Chemical Group), magnesium chloride hexahydrate (98.0%, Xilong Chemical Group), and aluminum chloride hexahydrate (97.0%, Sinopharm Chemical Reagent) of analytical grade were used without further purification in the experiments. Analytically pure NH_4OH was supplied by Beijing Chemical Plant with the concentration of 20–25%. Distilled water with specific conductivity (<0.1 μS cm^{-1}) was used.

Procedure for phase equilibria determination

A jacketed glass vessel with a volume of 250 mL and a condenser were used in this work as Figure 1 shows. A typical experimental procedure was performed as follows: The $AlCl_3$ solution with known concentration was put into the vessel, and the system was maintained at a desired temperature with ± 0.1 K using a thermostat. A known mass of NH_4Cl was added into the solution and agitation was provided by magnetic stirring. Some time later, if the last trace of solid was observed to disappear, more salt of known mass was added. All the chemical reagents were prepared by weighing the pure components with an uncertainty of ± 0.01 g.

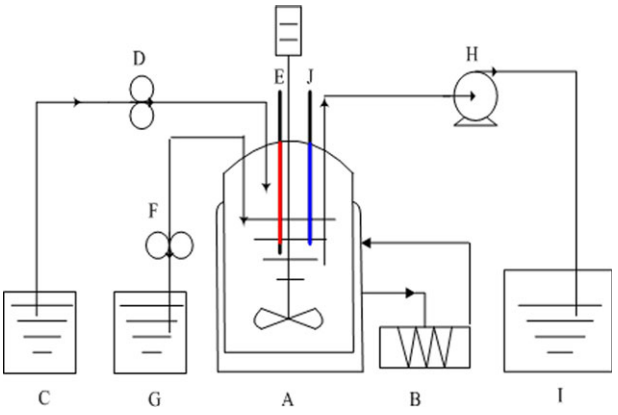

Figure 2. System applied for the coprecipitation experiments.

(A) MSMPR reactor; (B) water bath; (C) magnesium chloride solution tank; (D) peristaltic pump; (E) thermometer; (F) peristaltic pump; (G) alkali solution tank; (H) pump; (I) product; (J) electrode. [Color figure can be viewed in the online issue, which is available at wileyonlinelibrary.com.]

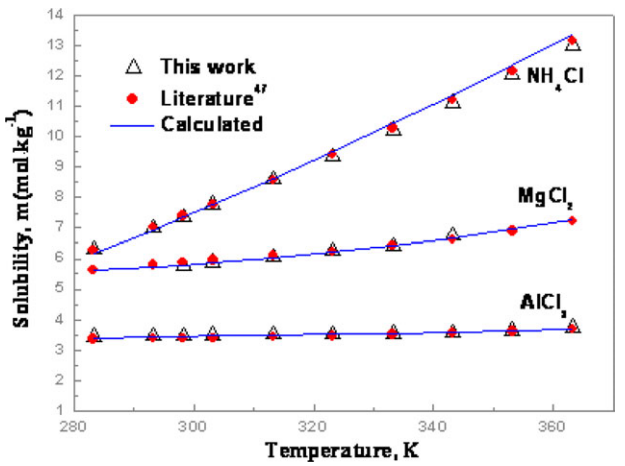

Figure 3. Solubility of NH_4Cl, $AlCl_3$ and $MgCl_2$ in the NH_4Cl-H_2O, $AlCl_3$-H_2O, and $MgCl_2$-H_2O binary system, respectively.

[Color figure can be viewed in the online issue, which is available at wileyonlinelibrary.com.]

Table 1. Chemical Species and Their Speciation Reactions in the NH_3-$MgCl_2$-$AlCl_3$-NH_4Cl-H_2O System with Aid of OLI Engine

Species	Dissociation reactions
H_2O	$H_2O = H^+ + OH^-$
$NH_4Cl(s)$	$NH_4Cl(s) = NH_4^+ + Cl^-$
$MgCl_2{\cdot}6H_2O(s)$	$MgCl_2{\cdot}6H_2O(s) = Mg^{2+} + 2Cl^- + 6H_2O$
$AlCl_3{\cdot}6H_2O(s)$	$AlCl_3{\cdot}6H_2O(s) = Al^{3+} + 3Cl^- + 6H_2O$
HCl(aq)	$HCl(aq) = H^+ + Cl^-$
$AlCl_3(aq)$	$AlCl_3(aq) = Al^{3+} + 3Cl^-$
$MgCl_2(aq)$	$MgCl_2(aq) = Mg^{2+} + 2Cl^-$
$AlO_2H_2Cl(aq)$	$AlO_2H_2Cl(aq) = Al^{3+}+2OH^- + Cl^-$
$Al(OH)_2^+$	$Al(OH)_2^+ = Al(OH)^{2+} + OH^-$
$Al(OH)_3(aq)$	$Al(OH)_3(aq) = Al(OH)_2^+ + OH^-$
$Al(OH)_4^-$	$Al(OH)_4^- = Al(OH)_3(aq) + OH^-$
$AlOH^{2+}$	$AlOH^{2+} = Al^{3+} + OH^-$
$AlOHCl^+$	$AlOHCl^+ = Al^{3+}+OH^- + Cl^-$
$Al(OH)_3(s)$	$Al(OH)_3(s) = Al^{3+} + 3OH^-$
Mg_4Al_2 $(OH)_{14}{\cdot}3H_2O(s)$	$Mg_4Al_2(OH)_{14}{\cdot}3H_2O(s) = 4Mg^{2+}$ $+ 2Al(OH)_4^-6OH^- + 3H_2O$

Experimental setup for coprecipitation

Figure 2 shows the sketch of the laboratory system applied for the coprecipitation experiments. The main part of experimental setup was a laboratory-scale continuous MSMPR reactor equipped with propeller agitator responsible for internal circulation of suspension. There was a jacketed glass reactor (A), inside which a three-paddle propeller mixer of standard geometrical proportions was located. The speed of the stirrer was kept at 300 rpm to satisfy the hydrodynamic requirements of maintaining a stable and intensive enough circulation of suspension inside the reactor working volume. The temperature of the solution in the reactor was held constant by the circulation of heating water from a water batch with a thermoelectric controller (B) through the jacket of the reactor. Using the digital peristaltic pumps (D) and (F), the NH_4OH solution was carried from tank (C) and $MgCl_2$-$AlCl_3$ solution (Mg/Al = 2) from tank (G) to the reactor, respectively. Sampling was carried out through a pump (H) working intermittently at high flow rate, and the slurry withdrawn was pumped to the product tank (I). Electrode (J) was used to measure the pH.

Experimental procedure

Coprecipitation was carried out in the MSMPR reactor mentioned above. The solution was preheated to the desired operating temperature, and then the two reactant solutions were continuously and simultaneously fed to the MSMPR reactor from their own inlet tubes located on opposite sides of the impeller with the same flow rate of 10 mL min^{-1}. In a typical run, once the working volume of the slurry within the reactor was achieved 400 mL, the slurry in the reactor was discharged intermittently by a peristaltic pump, and the withdrawal tube of product slurry was located approximately half way up the side of the reactor. Every slurry sample withdrawn from the reactor was 20–25 mL. The reactor was operated to reach steady state, which was found to be at least eight residence times (τ). After that, the coprecipitate was then collected, filtered off, washed with distilled water and ethanol three times to remove the ionic remnants, and dried slowly in an oven at 333.2 K for 12 h.

The structure and morphology of the coprecipitate were characterized by powder x-ray diffraction (XRD), scanning electron microscopy (SEM) (JEOL Model JSM-6700F). Powder XRD (X'Pert PRO MPD, PANalytical, Almelo, The Netherlands) patterns were recorded on a diffractometer (using Cu K_α radiation) operating at 40kV/30 mA. A scanning rate of 0.02/s was applied to record the patterns in the 2θ angle range of 5−90°. At last, a 20 mL sample of the slurry was withdrawn from the reactor for particle size distributions (PSDs) analysis using the Malvern Mastersizer of Hydro 2000 MU.

The obtained $Mg_4Al_2(OH)_{14}{\cdot}3H_2O$ was calcined at temperature from 773.2 to 1273.2 K for about 2 h to prepare Mg-Al spinel. The crystallinity and the morphology of the calcined powders were characterized via XRD analysis and SEM-EDS (ZEISS, EVO 18, Special Edition), respectively.

Chemical modeling framework

Chemistry of the NH_3-$MgCl_2$-$AlCl_3$-NH_4Cl-H_2O system. For the NH_3-$MgCl_2$-$AlCl_3$-NH_4Cl-H_2O system, there exist many species including NH_4^+, H^+, Mg^{2+}, Al^{3+}, Cl^- and various chemical equilibria among them (Table 1). The main dissociation reactions can be described as:

$$NH_4Cl(s) = NH_4^+ + Cl^- \tag{2}$$

$$MgCl_2 \cdot 6H_2O(s) = Mg^{2+} + 2Cl^- + 6H_2O \tag{3}$$

$$AlCl_3 \cdot 6H_2O(s) = Al^{3+} + 3Cl^- + 6H_2O \tag{4}$$

$$Mg_4Al_2(OH)_{14} \cdot 3H_2O(s) = 4Mg^{2+} + 2Al(OH)_4^- + 6OH^- + 3H_2O \tag{5}$$

Table 2. Relevant Thermodynamic Data of the NH_4Cl-$MgCl_2$-$AlCl_3$-H_2O System (From the Databank of the OLI Aqueous Thermodynamic Model)[32]

Species	$\Delta G^0_{f,298.15\,K}$ (kJ mol^{-1})	$\Delta H^0_{f,298.15\,K}$ (kJ mol^{-1})	$\Delta S^0_{f,298.15\,K}$ (J mol^{-1} K^{-1})	$\Delta C^0_{p,f,298.15\,K}$ (J mol^{-1} K^{-1})	$\Delta V^0_{f,298.15\,K}$ (cm^3 mol^{-1})	Source
H_2O	−237.295	−285.956	69.98	75.33	18.062	Ref. 33
NH_4^+	−79.4542	−133.260	111.169	65.8562	18.13	Ref. 31
Mg^{2+}	−454.161	−466.178	−138.16	−22.35	−21.6	Ref. 31
Al^{3+}	−483.914	−530.904	−325.24	−136.04	44.4	Ref. 34
Cl^-	−131.29	−167.08	56.735	−123.177	17.79	Ref. 31
$AlOH^{2+}$	−692.658	−767.358	−176.68	55.25	28.2	Ref. 34
$Al(OH)_2^+$	−899.455	−1001.343	−43.07	−50.23	17.79	Ref. 34
$Al(OH)_3$ (l)	−1106.689	−1238.145	90.91	−133.96	20.39	Ref. 34
$Al(OH)_4^-$	−1306.278	−1501.665	109.74	100.85	50.18	Ref. 34
$Al(OH)_3$ (s)	−1155.910	−1294.072	68.47	92.01	–	Ref. 34
$NH_4Cl(s)$	−203.092	−314.553	95.86	86.441	35.03	Ref. 35
$MgCl_2{\cdot}6H_2O(s)$	−2114.89	−2498.85	366.1	315.725	129.6	Ref. 36
$AlCl_3{\cdot}6H_2O(s)$	−2266.19	−2737.03	182.0769	296.23	100.6	Ref. 37
$Mg_4Al_2(OH)_{14}{\cdot}3H_2O(s)$	−6365.50	−7145.05	1241	−485	–	Ref. 18

The solubility product (equilibrium constant of each reaction above) is designated as K_1-K_4 for reactions 2-5, respectively. The calculations in this article will be molality-based equilibrium constants for the various species of interest, which are defined as follows:

$$K_1 = a_{NH_4^+} \cdot a_{Cl^-} = \gamma_{NH_4^+} \cdot m_{NH_4^+} \cdot \gamma_{Cl^-} \cdot m_{Cl^-} \quad (6)$$

$$K_2 = a_{Mg^{2+}} \cdot a_{Cl^-}^2 \cdot a_{H_2O}^6 = \gamma_{Mg^{2+}} \cdot m_{Mg^{2+}} \cdot \gamma_{Cl^-}^2 \cdot m_{Cl^-}^2 \cdot a_{H_2O}^6 \quad (7)$$

$$K_3 = a_{Al^{3+}} \cdot a_{Cl^-}^3 \cdot a_{H_2O}^6 = \gamma_{Al^{3+}} \cdot m_{Al^{3+}} \cdot \gamma_{Cl^-}^3 \cdot m_{Cl^-}^3 \cdot a_{H_2O}^6 \quad (8)$$

$$K_4 = a_{Mg^{2+}}^4 \cdot a_{Al(OH)_4^-}^2 \cdot a_{OH^-}^6 \cdot a_{H_2O}^3 = m_{Mg^{2+}}^4 \cdot m_{Al(OH)_4^-}^2 \cdot m_{OH^-}^6 \cdot \gamma_{Mg^{2+}}^4 \cdot \gamma_{Al(OH)_4^-}^2 \cdot \gamma_{OH^-}^6 \cdot a_{H_2O}^3 \quad (9)$$

where a_i, m_i, γ_i represent the activity, concentration in molality, and activity coefficient of species i, respectively.

Equilibrium constants

To obtain the dissociation reaction constants, the standard-state thermodynamic data of the equilibrium species are required.[29] The equilibrium constant K can be calculated by the following equations:

$$\ln K = -\frac{\Delta G_T^0}{RT} \quad (10)$$

where ΔG_T^0 represents the standard-state Gibbs free energy change of reaction at temperature T (in Kelvin), and R is the gas constant (8.3145 J mol^{-1} K^{-1}).

There are two alternative methods in OLI software applied to achieve this goal, including the HKF model[30,31] and the empirical equation. The HKF model was used to calculate the standard properties of aqueous species, and the relevant thermodynamic data at standard state are listed in Table 2. And empirical equation was adopted to calculate the solubility products of solids in this article as follows:

$$\log K = A + \frac{B}{T} + CT + DT^2 \quad (11)$$

where A, B, C, and D are empirical parameters. T is the temperature (in Kelvin). Eq. 11 may be applied to calculate the solubility product, and four parameters are obtained via fitting to experimental solubility data.

Aqueous activity coefficients

The calculation of activity and activity coefficients is associated with the solubility product (Eqs. 6–9) and supersaturation of the crystallization process.[38] The NH_3-$MgCl_2$-$AlCl_3$-NH_4Cl-H_2O system contains many ionic species such as NH_4^+, Mg^{2+}, Al^{3+}, and Cl^-, so the Bromley-Zemaitis model was used via the OLI platform.[32]

The Bromley-Zemaitis activity coefficient equation,[39] which represents only ion–ion interactions, was developed by Bromley[40] and empirically modified by Zemaitis.[41] This model has been widely adopted for electrolytes[42–46] with concentrations of 0–30 M at 0–473.15 K. The Bromley-Zemaitis activity coefficient equation for the case of cation i in a multicomponent electrolyte solution can be described as follows:

$$\log \gamma_i = \frac{-AZ_i^2\sqrt{I}}{1+\sqrt{I}} + \sum_j \left[\frac{(0.06+0.6B_{ij})|Z_iZ_j|}{\left(1+\frac{1.5I}{|Z_iZ_j|}\right)^2} + B_{ij} + C_{ij}I + D_{ij}I^2 \right] \times \left(\frac{|Z_i|+|Z_j|}{2}\right)^2 m_j \quad (12)$$

where j indicates all anions in solution, A is the Debye-Hückel parameter, I is the ionic strength of the solution, B, C, and D

Table 3. Experimental Solubilities in the NH_4Cl(s)-$AlCl_3$-H_2O System

m($AlCl_3$), mol kg^{-1}	m(NH_4Cl), mol kg^{-1}				
	T = 283.2 K	T = 293.2 K	T = 298.2 K	T = 303.2 K	T = 313.2 K
0	6.2907	6.9843	7.3572	7.7805	8.5934
0.4750	4.8487	5.5652	5.8791	6.2143	6.9184
0.9027	3.6916	4.3074	4.6415	4.9503	5.6454
1.2840	2.7825	3.3137	3.5681	3.9201	4.5425
1.6429	2.0059	2.4789	2.7492	2.9935	3.5878
1.9693	1.5892	2.0041	2.1800	2.4512	3.0112
2.2628	1.1691	1.5922	1.7488	2.0280	2.5301
2.4991	1.0492	1.4319	1.6074	1.8464	2.2310
2.7498	0.9552	1.2916	1.4374	1.6131	2.0187
2.9964	0.7349	1.0501	1.2590	1.4418	1.8185
	T = 323.2 K	T = 333.2 K	T = 343.2 K	T = 353.2 K	
0	9.3597	10.2304	11.1085	12.0557	
0.4750	7.7040	8.4099	9.1636	9.9652	
0.9027	6.3473	7.0981	7.8539	8.7212	
1.2840	5.2306	5.9186	6.6930	7.5474	
1.6429	4.2268	4.8872	5.6060	6.3816	
1.9693	3.5639	4.1870	4.8775	5.5958	
2.2628	3.0406	3.6089	4.2873	4.9882	
2.4991	2.7537	3.2653	3.8627	4.5012	
2.7498	2.4804	2.9758	3.5122	4.1067	
2.9964	2.2811	2.7008	3.2454	3.6259	

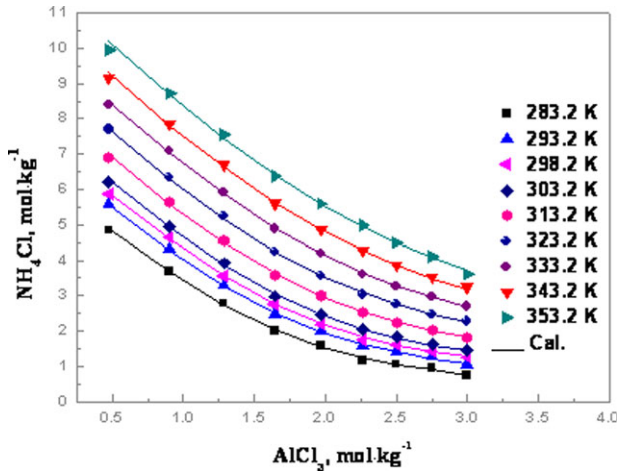

Figure 4. Phase equilibria data of the NH_4Cl-$AlCl_3$-H_2O system at temperature range from 283.2 to 353.2 K.

[Color figure can be viewed in the online issue, which is available at wileyonlinelibrary.com.]

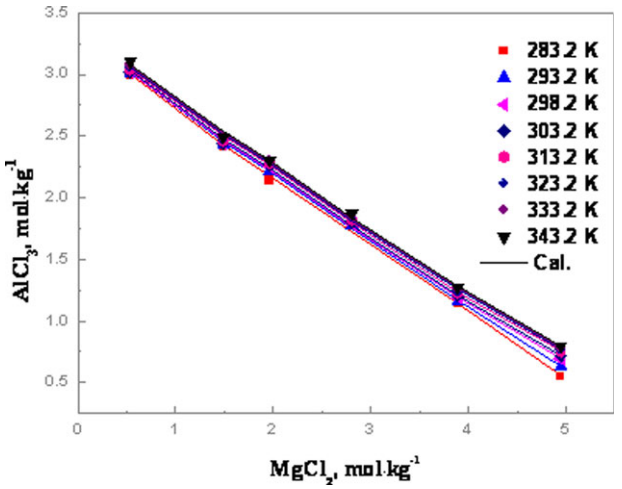

Figure 5. Phase equilibria data of the $AlCl_3$-$MgCl_2$-H_2O system at temperature range from 283.2 to 343.2 K.

[Color figure can be viewed in the online issue, which is available at wileyonlinelibrary.com.]

are temperature-dependent empirical coefficients, Z_i and Z_j are the cation and anion charges, respectively. Finally, the formulation of water activity[41] in a multicomponent system was adopted in OLI's thermodynamic framework.

Results and Discussion

Phase equilibria of the NH_4Cl-$MgCl_2$-$AlCl_3$-H_2O system

The validation of the solubility determination procedure proposed above was performed by comparing the experimental values with literature data. Figure 3 compares the solubility[47] of binary NH_4Cl-H_2O, $MgCl_2$-H_2O and $AlCl_3$-H_2O systems at 283.2–363.2 K. Good agreement between experimentally determined solubility in the present work and literature values was found with relative deviations of less than 0.5%, indicating the procedure is acceptable.

The solubility of NH_4Cl(s) in the NH_4Cl-$AlCl_3$-H_2O system was experimentally measured by use of method mentioned above from 283.2 to 353.2 K with the concentration of $AlCl_3$ from 0 to 3.0 mol kg^{-1}. The solubility data are tabulated in Table 3 and depicted in Figure 4. It is clear that the solubility of NH_4Cl increases with temperature over the investigated range. However, the solubility of NH_4Cl decreases gradually with an increase of the $AlCl_3$ molality up to 3 mol kg^{-1}.

For the ternary $AlCl_3$-$MgCl_2$-H_2O system, the measured $AlCl_3 \cdot 6H_2O$ solubility data are presented in Table 4 and plotted in Figure 5. As shown in Figure 5, the solubility of $AlCl_3$ decreases with an increase of the $MgCl_2$ molality, but increases a bit over the investigated temperature range in the presence of $MgCl_2$.

For the ternary NH_4Cl-$MgCl_2$-H_2O system, the NH_4Cl solubility data reported by Wang and Li[19] are displayed in Figure 6. These values will be used in model parameter regression in the following section.

Table 4. Experimental Solubilities in the $AlCl_3$(s)-$MgCl_2$-H_2O System

m($MgCl_2$), mol kg^{-1}	m($AlCl_3$), mol kg^{-1}	m($MgCl_2$), mol kg^{-1}	m($AlCl_3$), mol kg^{-1}	m($MgCl_2$), mol kg^{-1}	m($AlCl_3$), mol kg^{-1}
T = 283.2 K		T = 293.2 K		T = 298.2 K	
0.5345	2.9958	0.5333	3.0095	0.5326	3.0181
1.4888	2.4166	1.4864	2.4279	1.4845	2.4366
1.9635	2.1418	1.9422	2.2186	1.9339	2.2489
2.8092	1.7704	2.8060	1.7789	2.8031	1.7866
3.8924	1.1377	3.8801	1.1632	3.8698	1.1847
4.9461	0.5498	4.8980	0.6343	4.8633	0.6953
T = 303.2 K		T = 313.2 K		T = 323.2 K	
0.532	3.0243	0.5309	3.0371	0.5292	3.0570
1.4826	2.4452	1.4785	2.4642	1.4766	2.4728
1.9291	2.2662	1.9256	2.2789	1.9224	2.2904
2.7971	1.8026	2.7895	1.8228	2.7842	1.8370
3.8607	1.2036	3.8475	1.2311	3.8415	1.2436
4.8490	0.7205	4.8320	0.7505	4.8225	0.7671
T = 333.2 K		T = 343.2 K			
0.5277	3.0750	0.5256	3.0997		
1.4734	2.4873	1.4716	2.4958		
1.9208	2.2961	1.9193	2.3018		
2.7763	1.8578	2.7692	1.8769		
3.8332	1.2610	3.8273	1.2734		
4.8131	0.7836	4.8075	0.7935		

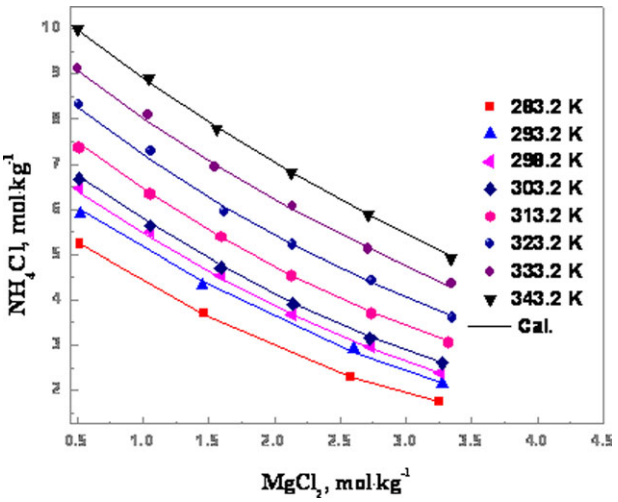

Figure 6. Phase equilibria data of the NH_4Cl-$MgCl_2$-H_2O system at temperature range from 283.2 to 343.2 K.

[Color figure can be viewed in the online issue, which is available at wileyonlinelibrary.com.]

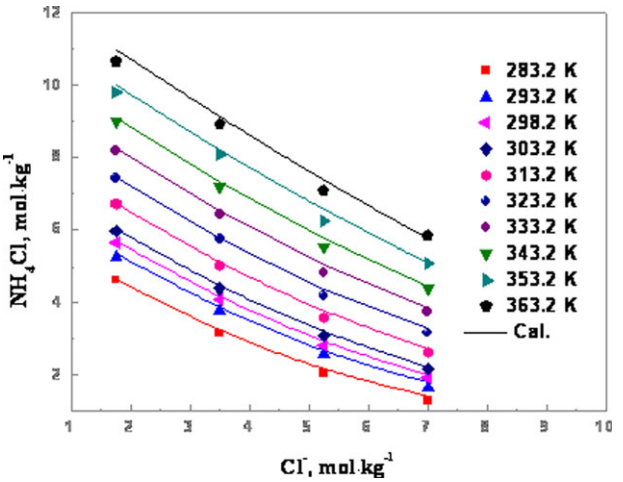

Figure 7. Phase equilibria data of the NH_4Cl-$MgCl_2$-$AlCl_3$-H_2O quaternary system from 283.2 to 363.2 K. Mole ratio Mg/Al = 2.

[Color figure can be viewed in the online issue, which is available at wileyonlinelibrary.com.]

For the quaternary NH_4Cl-$MgCl_2$-$AlCl_3$-H_2O system, the determined solubility of NH_4Cl in mixed $MgCl_2$-$AlCl_3$ solution (Mg/Al = 2) at 283.2–363.2 K is listed in Table 5 and shown in Figure 7. It is obvious that the solubility of NH_4Cl decreases sharply with the concentration of $MgCl_2$-$AlCl_3$ solutions.

Model parameterization

The capability of existing Bromley-Zemaitis model parameters for predicting the solubility should be tested before usage. The solubility data of binary NH_4Cl-H_2O, $MgCl_2$-H_2O, and $AlCl_3$-H_2O systems from 283.2 to 363.2 K are compared to model's prediction in Figure 3. As shown in Figure 3,the existing model gives good results for the solubility of binary systems. However, the solubility of ternary systems including NH_4Cl-$AlCl_3$-H_2O, $AlCl_3$-$MgCl_2$-H_2O, and NH_4Cl-$MgCl_2$-H_2O cannot be predicted well with the existing interaction parameters. Therefore, new Bromley-Zemaitis model parameters for ion–ion interaction (such as NH_4^+-Cl^-, Al^{3+}-Cl^-, NH_4^+-Al^{3+}, NH_4^+-Mg^{2+} and Mg^{2+}-Al^{3+}), and K_3 were determined via regression of the solubility of the ternary systems obtained in this work and the literature.[19] In this regression, the model parameters were obtained by minimizing the sum of squared deviations between the experimental and calculated values of solubility. The newly obtained parameters are listed in Table 6. The newly obtained K_3 is presented in Table 7 with K_1 and K_2 from the OLI default databank.

After obtaining new model parameters and K_3, the regressed results are demonstrated in Figures 4–6, respectively. As can be seen, all the regressed solubility data agree well with the experimental values. Figures 8–10 show that most of the deviations for the ternary NH_4Cl-$AlCl_3$-H_2O, $AlCl_3$-$MgCl_2$-H_2O, and NH_4Cl-$MgCl_2$-H_2O systems are less than 5%.

The validation of the newly obtained parameters was then performed by predicting the solubilities of the quaternary NH_4Cl-$MgCl_2$-$AlCl_3$-H_2O system that were not used in the regression stage. The comparison of the predictions and experimental results from 283.2 to 363.2 K in this work is depicted in Figure 7. As can be seen from Figure 11, most of deviations are less than 5% with few data points at 283.2 K exhibiting the maximum deviation of 10.7%. The predictions are in good agreement with experimental values, indicating that the newly obtained Bromley-Zemaitis model parameters reasonably represent the NH_4Cl solubility of the quaternary NH_4Cl-$MgCl_2$-$AlCl_3$-H_2O system over the studied temperature range.

Effect of parameters on coprecipitation

The particle size and PSD can affect many properties of solid particles,[48] such as filtration characteristics. To produce $Mg_4Al_2(OH)_{14}{\cdot}3H_2O$ with excellent filterability, the influence of parameters on the coprecipitation, including temperature,

Table 5. Experimental Solubilities in the NH_4Cl(s)-$MgCl_2$-$AlCl_3$-H_2O System

m($MgCl_2$), mol kg^{-1}	m($AlCl_3$), mol kg^{-1}	m(NH_4Cl), mol kg^{-1}				
		T = 283.2 K	T = 293.2 K	T = 298.2 K	T = 303.2 K	T = 313.2 K
0.4992	0.2501	4.6342	5.2853	5.6696	5.9905	6.7293
0.9979	0.4989	3.1585	3.8078	4.1100	4.4029	5.0447
1.4992	0.7496	2.0700	2.5875	2.8359	3.1012	3.6075
1.9876	0.9929	1.2959	1.6523	1.9234	2.1740	2.6437
		T = 323.2 K	T = 333.2 K	T = 343.2 K	T = 353.2 K	T = 363.2 K
0.4992	0.2501	7.4457	8.1826	9.0017	9.8244	10.6658
0.9979	0.4989	5.7536	6.4532	7.2200	8.0820	8.9346
1.4992	0.7496	4.2035	4.8386	5.5411	6.2529	7.0861
1.9876	0.9929	3.1747	3.7613	4.4055	5.0924	5.8610

Table 6. Newly Obtained Bromley-Zemaitis Model Parameters For NH_4^+-Cl^-, Al^{3+}-Cl^-, NH_4^+-Al^{3+}, NH_4^+-Mg^{2+}, and Mg^{2+}-Al^{3+} Interactions

	Interactions				
Parameters	NH_4^+-Cl^-	$A1^{3+}$-Cl^-	NH_4^+-Al^{3+}	NH_4^+-Mg^{2+}	Mg^{2+}-$A1^{3+}$
B1	8.666E-02	−1.177E-02	0.12332	8.544E-02	−0.332476
B2	3.382E-03	2.296E-03	−1.065E-02	−1.890E-02	2.012E-04
B3	−2.409E-05	−6.547E-05	6.759E-05	4.358E-04	2.031E-05
C1	−2.006E-02	−7.702E-04	4.292E-03	−1.144E-02	8.966E-02
C2	−8.429E-04	−7.536E-04	2.138E-03	2.797E-03	3.833E-04
C3	2.286E-06	2.436E-06	−1.170E-05	−6.612E-05	6.194E-06
D1	1.188E-03	5.255E-04	−1.089E-03	−1.444E-04	−3.891E-03
D2	7.490E-05	2.734E-05	−1.132E-04	−1.315E-04	−1.863E-05
D3	−3.752E-07	6.022E-08	5.180E-07	2.523E-06	−4.063E-07

feed concentration, and addition of NH_4Cl was investigated using the MSMPR reactor.

Effect of temperature

The effect of temperature on the coprecipitation was studied from 303.2 to 343.2 K in mixed $MgCl_2$-$AlCl_3$ solution with mole ratio Mg/Al = 2 (initial concentrations of $MgCl_2$: 0.20, 1.00, and 2.00 mol kg^{-1}). The XRD observation of the particles prepared at different conditions is shown in Figure 12. It is clear that all the coprecipitates obtained from MSMPR reactor are confirmed to be $Mg_4Al_2(OH)_{14}{\cdot}3H_2O$. As can be seen from SEM images corresponding to the $Mg_4Al_2(OH)_{14}{\cdot}3H_2O$ samples prepared at reaction temperatures 303.2, 323.2, and 343.2 K(Figure 13a–c), rosette-like particles were obtained.

Figure 14 presents the PSDs of $Mg_4Al_2(OH)_{14}{\cdot}3H_2O$ crystals obtained at various temperatures and concentrations. The mean size of 30 μm (a)–(c), 10 μm (d)–(f), and 10 μm (g)–(i) shows that the temperature had little effect on the PSD of $Mg_4Al_2(OH)_{14}{\cdot}3H_2O$ particles obtained at the same concentration of $MgCl_2$-$AlCl_3$ solution.

Effect of feed concentration

Variable initial concentrations of 0.20, 1.00, and 2.00 mol kg^{-1} $MgCl_2$ were investigated from mixed $MgCl_2$-$AlCl_3$ solutions (mole ratio of Mg/Al = 2) at 303.2–343.2 K. Figure 13 shows that the obtained $Mg_4Al_2(OH)_{14}{\cdot}3H_2O$ particles always present rosette-like morphology with increasing concentration.

It can be seen from Figure 14 that the PSDs of $Mg_4Al_2(OH)_{14}{\cdot}3H_2O$ particles obtained from (d)–(i) are irregular, and the spans, $(D_{0.9}-D_{0.1})/D_{0.5}$, are high. The curves (a)–(c) are very close to a normal curve, and the size distribution (span) is sharpened. Therefore, the $Mg_4Al_2(OH)_{14}{\cdot}3H_2O$ crystals obtained at low concentration of $MgCl_2$-$AlCl_3$ solution (C_{Mg} = 0.20 mol kg^{-1}; C_{Al} = 0.10 mol kg^{-1}) over the temperature range from 303.2–343.2 K have the largest average size of 30 μm and the narrowest size distribution, resulting in better filtration characteristics.

Effect of NH_4Cl addition

The effect of NH_4Cl addition (1.00, 2.00, and 3.00 mol kg^{-1}) on the morphology and PSD of particles was investigated from mixed $MgCl_2$-$AlCl_3$ solution with C_{Mg} = 0.2 mol kg^{-1} and C_{Al} = 0.1 mol kg^{-1} at 343.2 K, and is depicted in Figures 15 and 16, respectively. From Figure 15j–l, the rosette-like shaped crystals are observed, indicating that the addition of NH_4Cl solution had a little effect on the microstructure of $Mg_4Al_2(OH)_{14}{\cdot}3H_2O$. The mean size of particles decreases a little bit from 35.13 to 29.11 μm with increasing NH_4Cl concentration in Figure 16.

Recovery of NH_4Cl by feeding $MgCl_2$-$AlCl_3$

The recovery of NH_4Cl was successfully performed in batch crystallization by using a 2-L jacketed stirred glass reactor. First, an NH_4Cl-rich solution of 4.0 mol kg^{-1} at 343.2 K was introduced into the vessel under a stirring speed of 200 rpm. And then, the mixed saturated $MgCl_2$-$AlCl_3$ solution (Mg/Al = 2) was fed into the crystallizer until the Mg^{2+} concentration reached 2.0 mol kg^{-1}. After that, the solution was cooled at a slow rate[49] by circulating water through the jacket. When the temperature decreased to 298.2 K, the NH_4Cl was crystallized and recovered in the cooling process.

The SEM images of recovered NH_4Cl are shown in Figure 17. The final product of NH_4Cl crystallizes well with a size of around 20 μm. After recovering NH_4Cl, an $MgCl_2$-$AlCl_3$-NH_4Cl solution was obtained and served as the feed for $Mg_4Al_2(OH)_{14}{\cdot}3H_2O$ coprecipitation by recycling into the next loop.

Preparation of Mg-Al spinel

The Mg-Al spinel was prepared by calcination of $Mg_4Al_2(OH)_{14}{\cdot}3H_2O$ at temperature from 773.2 to 1273.2 K for 2 h in a muffle furnace. The main reaction occurred as following:

$$Mg_4Al_2(OH)_{14}\cdot 3H_2O \rightarrow MgAl_2O_4 + 3MgO + 10H_2O \quad (13)$$

Figure 18 displays the typical XRD patterns of the as-prepared spinel samples. It can be seen that the peaks are in

Table 7. Coefficients for Solubility Product Constants of $NH_4Cl(s)$, $MgCl_2{\cdot}6H_2O(s)$, $AlCl_3{\cdot}6H_2O(s)$, and $Mg_4Al_2(OH)_{14}{\cdot}3H_2O(s)$, Respectively

Parameters	A	B	C	D	T (K) range	Source
log K_1	−3.787	0	0.023471	-2.2060×10^{-5}	273.2–373.2	OLI databank
log K_2	−31.6216	4055.7	0.107410	-1.0585×10^{-4}	273.2–373.2	OLI databank
log K_3	10.0333	1573.4	0.013204	-1.6306×10^{-4}	273.2–373.2	This work
log K_4	−74.659	7603.6	0	0	273.2–373.2	OLI databank

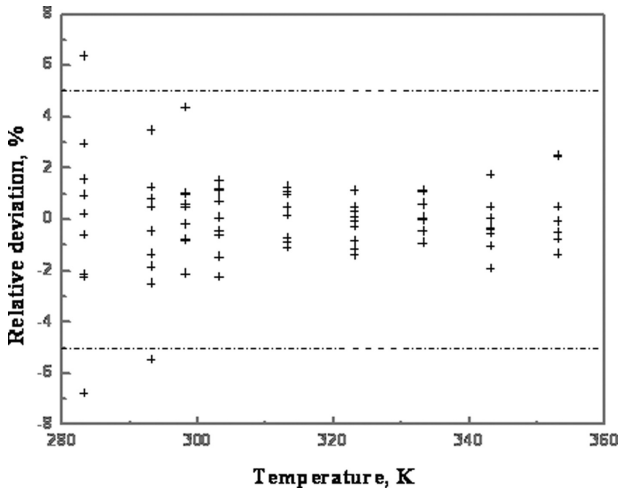

Figure 8. Relative deviation of the calculated values for the phase equilibria data of the NH_4Cl-$AlCl_3$-H_2O ternary system.

The dash-dot line represents the relative deviation of ±5%.

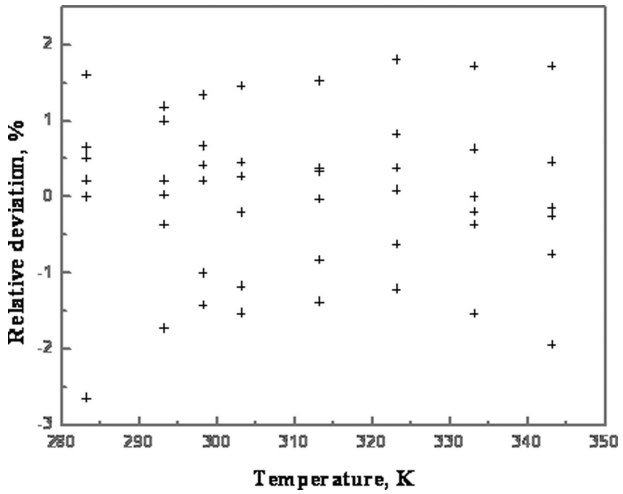

Figure 9. Relative deviation of the calculated values for the phase equilibria data of the $AlCl_3$-$MgCl_2$-H_2O ternary system.

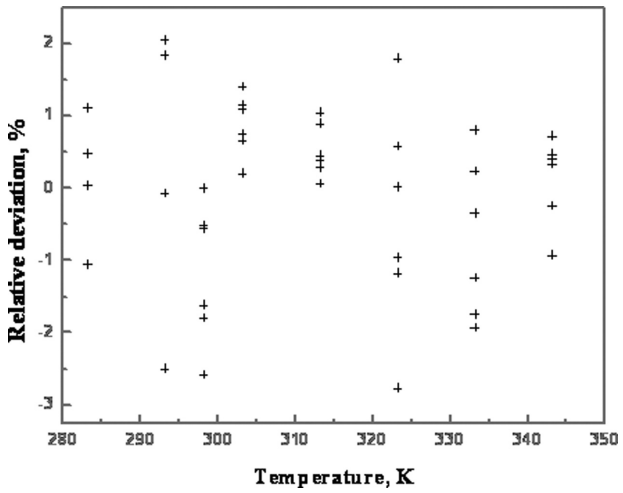

Figure 10. Relative deviation of the calculated values for the phase equilibria data of the NH_4Cl-$MgCl_2$-H_2O ternary system.

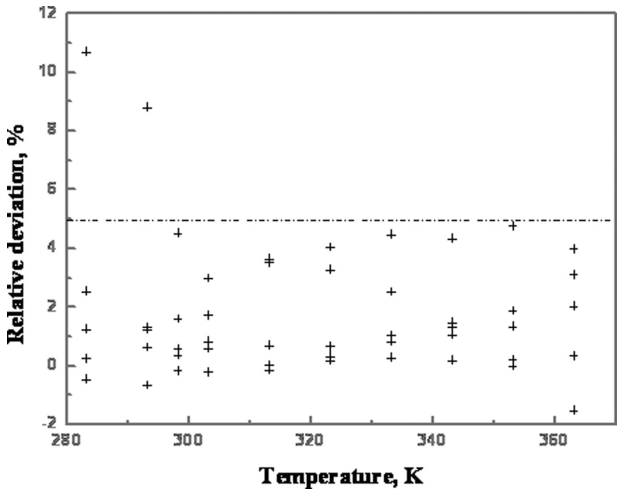

Figure 11. Relative deviation of the calculated values for the phase equilibria data of the NH_4Cl-$MgCl_2$-$AlCl_3$-H_2O quaternary system.

The dash-dot line represents the relative deviation of ±5%.

good agreement with the literature.[50] The temperature of Mg-Al spinel formation is only 773.2 K, much lower than the conventional oxide mixing (solid–solid reaction) method.[51,52] With increasing calcination temperature, the diffraction peaks of the spinel became sharper because the fraction of the spinel phase and its grain growth were enhanced at elevated temperatures up to 1273.2 K.

A set of typical SEM-EDS images of spinel samples is shown in Figure 19. The SEM-EDS analysis indicates that

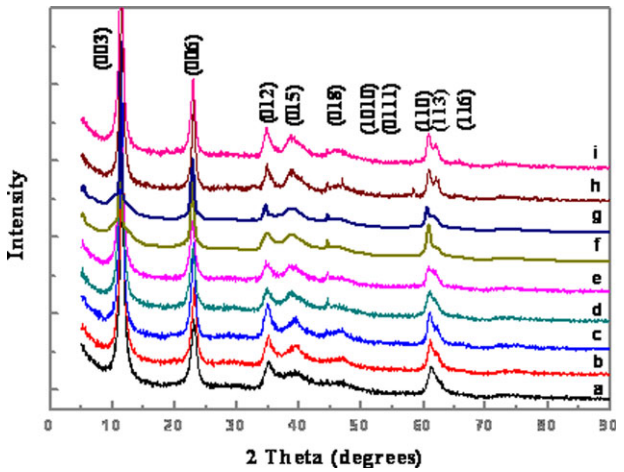

Figure 12. Effect of different reaction conditions on the XRD pattern of coprecipitates.

(a) 303.2 K, C_{Mg} = 0.20 mol kg^{-1}, C_{Al} = 0.10 mol kg^{-1}; (b) 323.2 K, C_{Mg} = 0.20 mol kg^{-1}, C_{Al} = 0.10 mol kg^{-1}; (c) 343.2 K, C_{Mg} = 0.20 mol kg^{-1}, C_{Al} = 0.10 mol kg^{-1}; (d) 303.2 K, C_{Mg} = 1.00 mol kg^{-1}, C_{Al} = 0.50 mol kg^{-1}; (e) 323.2 K, C_{Mg} = 1.00 mol kg^{-1}, C_{Al} = 0.50 mol kg^{-1}; (f) 343.2 K, C_{Mg} = 1.00 mol kg^{-1}, C_{Al} = 0.50 mol kg^{-1}; (g) 303.2 K, C_{Mg} = 2.00 mol kg^{-1}, C_{Al} = 1.00 mol kg^{-1}; (h) 323.2 K, C_{Mg} = 2.00 mol kg^{-1}, C_{Al} = 1.00 mol kg^{-1}; (i) 343.2 K, C_{Mg} = 2.00 mol kg^{-1}, C_{Al} = 1.00 mol kg^{-1}. [Color figure can be viewed in the online issue, which is available at wileyonlinelibrary.com.]

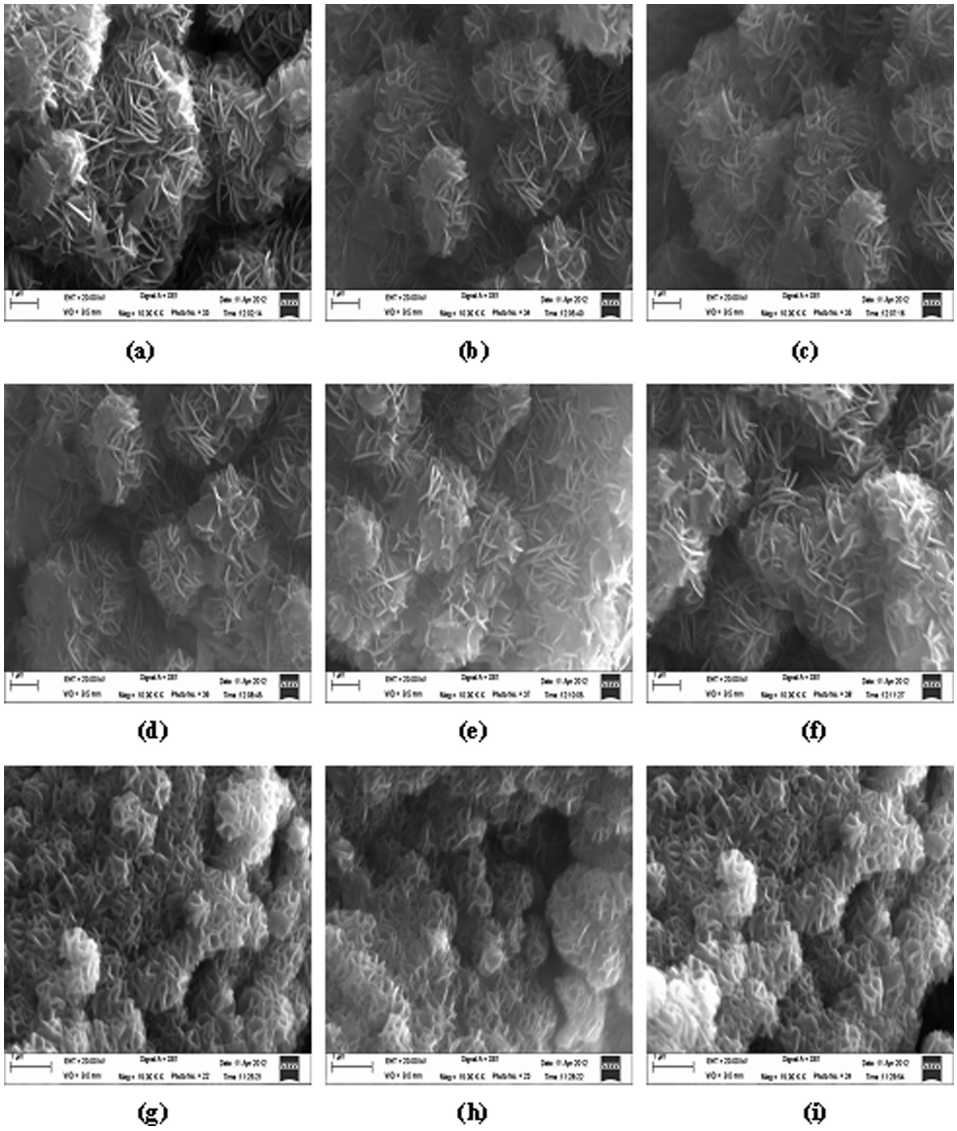

Figure 13. Typical SEM morphologies for the $Mg_4Al_2(OH)_{14}{\cdot}3H_2O$ prepared at different conditions.

the rosette-like particles were MgO mixed with $MgAl_2O_4$ at temperature from 773.2 to 1073.2 K. With increasing temperature, the partial MgO transformed to the irregular bulk while the left is still a mixture of MgO and $MgAl_2O_4$ at 1273.2 K.

The obtained spinel product has a chemical composition of 61% m/m MgO and 39% m/m Al_2O_3. According to the classifications of the magnesia spinel established by the International Organization for Standardization[53] (ISO) (Table 8), the sample satisfied the requirement of commercial spinel material, indicating a potentially commercial product from eventual industrial application.

Preliminary testing of a new process for Mg-Al spinel production

In light of the experimental results mentioned above, a practical approach to produce Mg-Al spinel with recovery of NH_4Cl was developed as shown in Figure 20. The

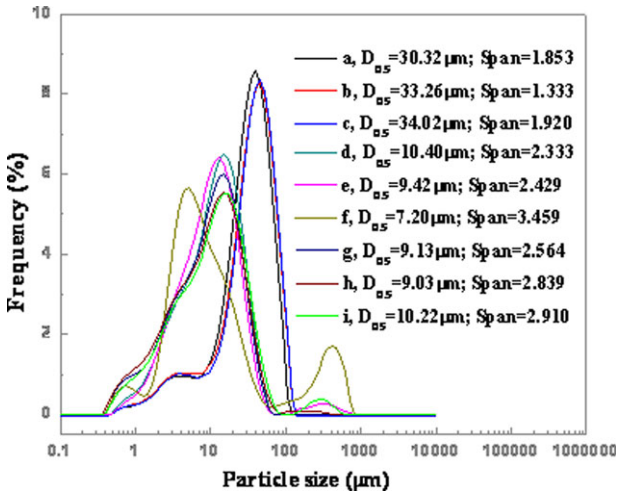

Figure 14. Effect of different conditions on the particle size distributions of $Mg_4Al_2(OH)_{14}{\cdot}3H_2O$.

[Color figure can be viewed in the online issue, which is available at wileyonlinelibrary.com.]

conceptual flow sheet consists of three main interlinked stages: coprecipitation of magnesium and aluminum from mixed $MgCl_2$-$AlCl_3$ solutions; calcination of the $Mg_4Al_2(OH)_{14}\cdot 3H_2O$ to Mg-Al spinel; and the recovery of NH_4Cl using common ion effect by feeding $MgCl_2$-$AlCl_3$. After recovering NH_4Cl, a $MgCl_2$-$AlCl_3$-rich solution was obtained and served as the feed for $Mg_4Al_2(OH)_{14}\cdot 3H_2O$ coprecipitation by recycling into the next cycle.

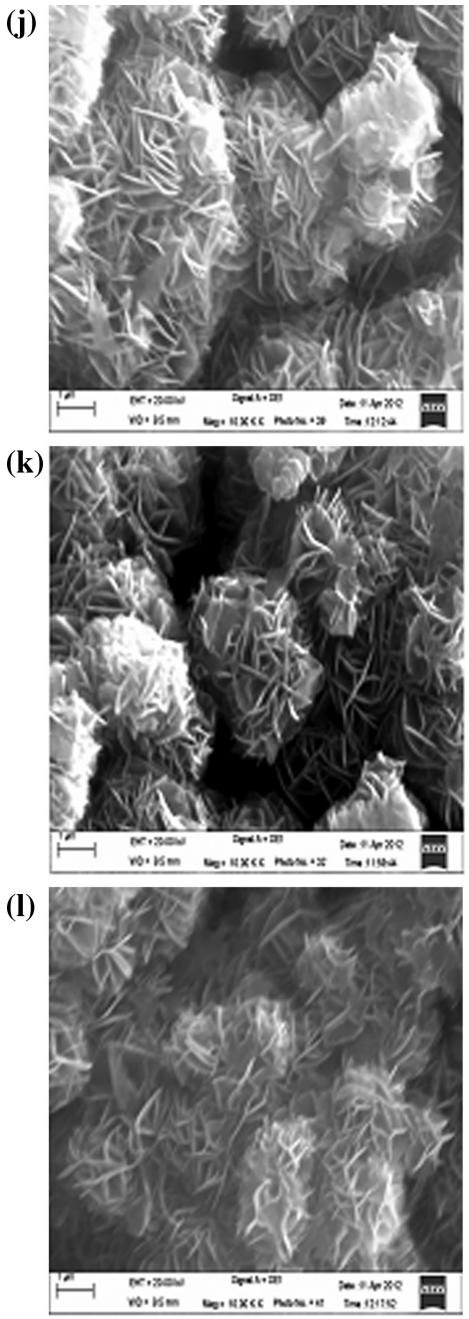

Figure 15. Typical SEM morphologies for the $Mg_4Al_2(OH)_{14}\cdot 3H_2O$ prepared at 343.2 K with NH_4Cl concentration from 1.00 to 3.00 mol kg^{-1}.

(j) C_{Mg} = 0.20 mol kg^{-1}, C_{Al} = 0.10 mol kg^{-1}, C_{NH_4Cl} = 1.00 mol kg^{-1}; (k) C_{Mg} = 0.20 mol kg^{-1}, C_{Al} = 0.10 mol kg^{-1}, C_{NH_4Cl} = 2.00 mol kg^{-1}; (l) C_{Mg} = 0.20 mol kg^{-1}, C_{Al} = 0.10 mol kg^{-1}, C_{NH_4Cl} = 3.00 mol kg^{-1}.

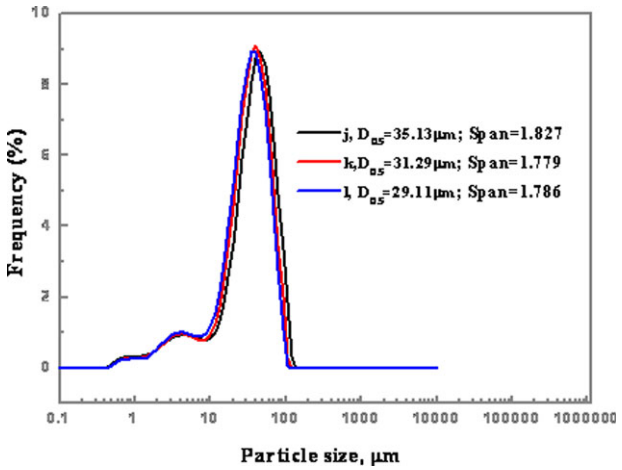

Figure 16. Effect of NH_4Cl addition on the PSDs of $Mg_4Al_2(OH)_{14}\cdot 3H_2O$ prepared at 343.2 K.

[Color figure can be viewed in the online issue, which is available at wileyonlinelibrary.com.]

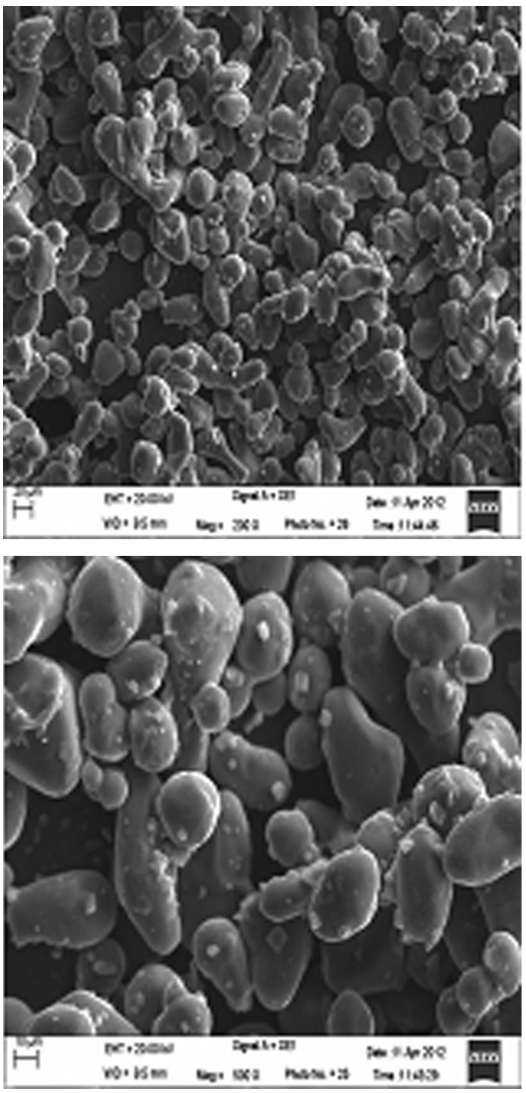

Figure 17. SEM patterns of ammonium chloride crystal recovered by feeding $MgCl_2$-$AlCl_3$.

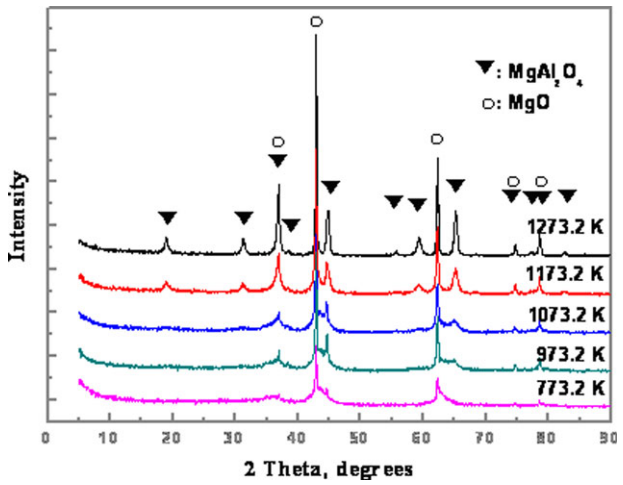

Figure 18. Effect of calcination temperature on the XRD pattern of Mg-Al spinel product.

[Color figure can be viewed in the online issue, which is available at wileyonlinelibrary.com.]

The $MgAl_2O_4$ product generated through this flowsheet has been successfully tested in a batch-wise fashion in the laboratory. The mass balances for the main components including $MgCl_2{\cdot}6H_2O$, $AlCl_3{\cdot}6H_2O$, NH_4Cl, and Mg-Al spinel were obtained and are shown in Figure 20. Hence, the preliminary technical feasibility of the above described process was demonstrated.

Table 8. ISO's Classification of Magnesia Spinel Products[53]

Types	Groups [MgO (% m/m)]					
Magnesia spinel	80	70	60	50	40	30
This work			61			

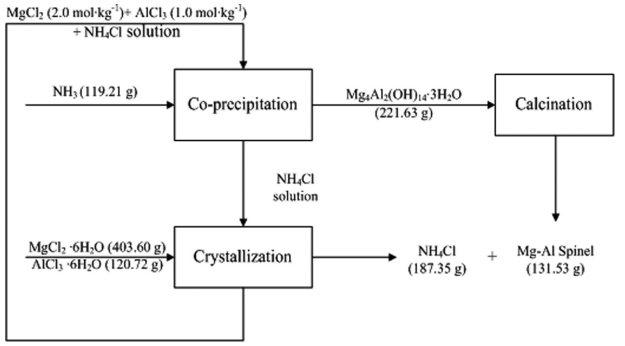

Figure 20. Illustrative flowsheet of the proposed practical approach to produce Mg-Al spinel.

Conclusions

A practical approach to produce Mg-Al spinel based on modeling of phase equilibria for NH_4Cl-$MgCl_2$-$AlCl_3$-H_2O system was proposed and proven feasible in this work.

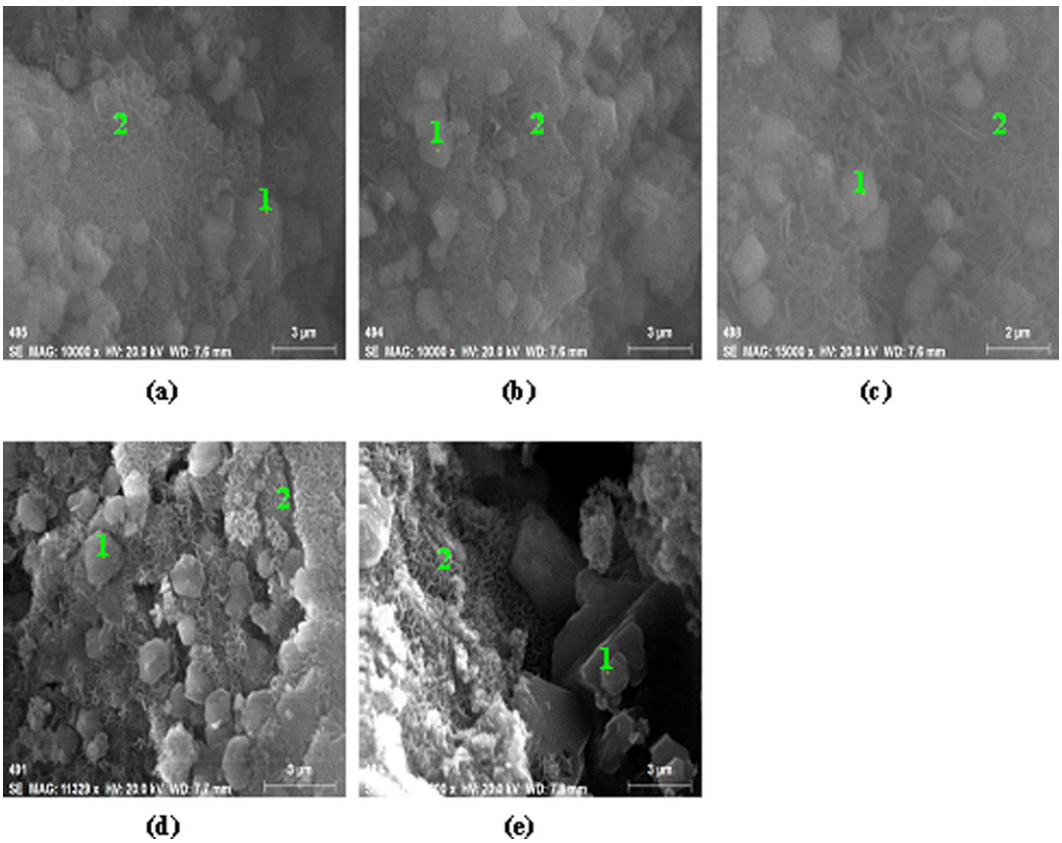

Figure 19. Typical SEM-EDS analysis for the Mg-Al spinel product prepared at temperature from 773.2 to 1273.2 K.

(a) 773.2 K, area 1, 2: $MgO+MgAl_2O_4$; (b) 973.2 K, area 1, 2: $MgO+MgAl_2O_4$; (c) 1073.2 K, area 1, 2: $MgO+MgAl_2O_4$; (d) 1173.2 K, area 1, 2: $MgO+MgAl_2O_4$; (e) 1273.2 K, area 1: MgO; area 2: $MgO+MgAl_2O_4$. [Color figure can be viewed in the online issue, which is available at wileyonlinelibrary.com.]

The phase equilibria of the NH_4Cl-$MgCl_2$-$AlCl_3$-H_2O system were determined over the temperature range from 283.2 to 363.2 K. The Bromley-Zemaitis model was adopted to represent the solubility of the quaternary system. The newly obtained Bromley-Zemaitis model parameters accurately predicted the phase equilibria of the quaternary system. The proposed process has been successfully tested in a continuous loop. The precursor $Mg_4Al_2(OH)_{14}\cdot 3H_2O$ was prepared from $MgCl_2$-$AlCl_3$ solutions (Mg/Al = 2) through investigating the influence of parameters on reaction in a MSMPR reactor. After filtration, high quality Mg-Al spinel products were obtained by calcination of a precursor at 773.2–1273.2 K. The NH_4Cl was also successfully recovered from the generated NH_4Cl-rich solution by $MgCl_2$-$AlCl_3$ addition.

Acknowledgments

The authors are grateful to the financial support of National Natural Science Foundation of China (21076213, 21076212 and 21146006), Key Program in Science & Technology of Qinghai Province (Grant 2010-G-A4), and National Basic Research Program of China (973 Program, 2009CB219904).

Notation

a = the activity
A = Debye-Hückel parameter; empirical parameter of log K
B = parameter of Bromley-Zemaitis equation; empirical parameter of log K
C = parameter of Bromley-Zemaitis equation; empirical parameter of log K
D = parameter of Bromley-Zemaitis equation; empirical parameter of log K
$D_{0.1}$ = the value of the particle diameter at 10% in the particle size distribution
$D_{0.5}$ = the value of the particle diameter at 50% in the particle size distribution
$D_{0.9}$ = the value of the particle diameter at 90% in the particle size distribution
G^0 = standard-state Gibbs free energy, J mol^{-1}
I = ionic strength
K = equilibrium constant
K_1 = solubility product for NH_4Cl(s)
K_2 = solubility product for $MgCl_2\cdot 6H_2O$(s)
K_3 = solubility product for $AlCl_3\cdot 6H_2O$(s)
K_4 = solubility product for $Mg_4Al_2(OH)_{14}\cdot 3H_2O$(s)
m_i = the molality of species i, mol kg^{-1}
R = universal gas constant, 8.3145 J mol^{-1} K^{-1}
T = absolute temperature, K
Z = the cation or anion charge

Greek letters

γ = compound activity coefficient

Subscripts and superscripts

i = specie
j = specie
exp = the experimental data
0 = standard state

Literature Cited

1. Zhang D, Zhou CH, Lin CX, Tong DS, Yu WH. Synthesis of clay minerals. *Appl Clay Sci*. 2010;50:1–11.
2. Ahmaruzzaman M. A review on the utilization of fly ash. *Prog Energy Combust Sci*. 2010;36:327–363.
3. Burkin AR. *Production of Aluminum and Alumina*. New Jersey: Wiley, 1987.
4. Izquierdo M, Querol X. Leaching behaviour of elements from coal combustion fly ash: an overview. *Int J Coal Geol*. 2011;94:54–66.
5. Ngagib S, Inoue K. Recovery of lead and zinc from fly ash generated from municipal incineration plants by means of acid and/or alkaline leaching. *Hydrometallurgy*. 2000;56:269–292.
6. Wang J, Ban H, Teng XJ, Wang H, Ladwig K. Impact of pH and ammonia on the leaching of Cu(II) and Cd(II) from coal fly ash. *Chemosphere*. 2006;64:1892–1898.
7. Rattanasak U, Chindaprasirt P. Influence of NaOH solution on the synthesis of fly ash geopolymer. *Miner Eng*. 2009;22:1073–1078.
8. Seidel A, Sluszny A, Shelef G, Zimmels Y. Self inhibition of aluminum leaching from coal fly ash by sulfuric acid. *Chem Eng J*. 1999;72:195–207.
9. Matjie RH, Bunt JR, van Heerden JHP. Extraction of alumina from coal fly ash generated from a selected low rank bituminous South African coal. *Miner Eng*. 2005;18:299–310.
10. Blanco F, Garcia MP, Ayala J. Variation in fly ash properties with milling and acid leaching. *Fuel*. 2005;84:89–96.
11. Bengtson KB, Chaberka P, Malm LE, Nunn RF, Stein DL. Alumina process feasibility study and preliminary pilot plant design. Task 1 report: comparison of six processes. BuMines Open File Rept. Pb-286 638. 1977:267.
12. Peters FA, Johnson PW. Revised and updated cost estimates for producing alumina from domestic raw materials. *BuMines IC 8648*. 1974:51.
13. Bengtson KB, Chaberka P, Nunn RF, San Jose AV, Manarolls GM, Malm LE. Alumina process feasibility study and preliminary pilot plant design. Task 3 report: Preliminary design of 25 ton per day pilot plant, vol. 1, Process Technology and Costs. BuMines Open File Rept. PB81-125301. 1979:231.
14. Eisele JA. Producing alumina from clay by the hydrochloric acid process, a bench-scale study. *BuMines RI 8476*. 1980:20.
15. Maysilles JH, Traut DE, Sawyer DL Jr. Aluminum chloride hexahydrate crystallization by HCl gas sparging, alumina recovery by the clay/hydrochloric acid process. *BuMines RI 8590*. 1984:20.
16. Poppleton HO, Sawyer DL. *Hydrochloric acid leaching of calcined kaolin to produce alumina*. In: Higbie KB, editor. *Light Metals, 1977*. Warrendale, PA: Metallurgical Society of AIME, 1977:103–114.
17. Shanks DE, Eisele JA, Bauer DJ. Hydrogen chloride sparging crystallization of aluminum chloride hexahydrate. *BuMines RI 8593*. 1981:15.
18. Eiseie JA, Bauer DJ, Shanks DE. Bench-scale studies to recover alumina from clay by a hydrochloric acid process. *Ind Eng Chem Prod Res Dev*. 1983;22:105–110.
19. Wang DG, Li ZB. Modeling solid-liquid equilibrium of NH_4Cl-$MgCl_2$-H_2O system and its application to recovery of NH_4Cl in MgO production. *AIChE J*. 2011;57:1595–1606.
20. Zhang S, Lee WE. *Spinel-containing refractories*. In Schacht CA. editor. *Refractories Handbook*. New York: Marchel Dekker Inc, 2004.
21. Shulman A, Linderholm C, Mattisson T, Lyngfelt A. High reactivity and mechanical durability of $NiO/NiAl_2O_4$ and $NiO/NiAl_2O_4$/$MgAl_2O_4$ oxygen carrier particles used for more than 1000 h in a 10 kW CLC reactor. *Ind Eng Chem Res*. 2009;48:7400–7405.
22. Mattisson T, Leion H, Lyngfelt A. Chemical-looping with oxygen uncoupling using CuO/ZrO_2 with petroleum coke. *Fuel*. 2009;88:683–690.
23. Iggland M, Leion H, Mattisson T, Lyngfelt A. Effect of fuel particle size on reaction rate in chemical looping combustion. *Chem Eng Sci*. 2010;65:5841–5851.
24. Bratton RJ. Coprecipitates yielding $MgAl_2O_4$ spinel powders. *Am Ceram Soc Bull*. 1969;48:759–762.
25. Hemrick JG, Smith JD, O'Hara K, Colavito D, Rodrigues-Schroer A. Novel spinel-family refractories for high-temperature, high-alkaline environments. In: 49th Conference of Metallurgists. 2010:67–80.
26. Gao WC, Li ZB. Solubility and K_{SP} of $Mg_4Al_2(OH)_{14}\cdot 3H_2O$ at the various ionic strengths. *Hydrometallurgy*. 2012;117–118:36–46.
27. Hou TP. *Soda Engineering*. Beijing: Chemical Engineering Press, 1959.
28. Christov C. Thermodynamic study of the K-Mg-Al-Cl-SO_4-H_2O system at the temperature 298.15 K. *Calphad*. 2001;25:445–454.
29. Ji XY, Lu XH, Zhang LZ, Bao NZ, Wang YR, Shi J, Lu Benjamin CY. A further study of solid-liquid equilibrium for the NaCl-NH_4Cl-H_2O system. *Chem Eng Sci*. 2000;55:4993–5001.
30. Helgeson HC, Kirkham DH, Flowers GC. Theoretical prediction of the thermodynamic behavior of aqueous electrolytes at high pressures and temperatures. IV. Calculation of activity coefficients,

osmotic coefficients, and apparent molar and standard and relative partial molar properties to 600°C and 5 kb. *Am J Sci*. 1981;281:1249–1516.
31. Shock EL, Helgeson HC. Calculation of the thermodynamic and transport properties of aqueous species at high pressures and temperatures: Correlation algorithms for ionic species and equation of state predictions to 5 kb and 1000°C. *Geochim Cosmochim Acta*. 1988;52:2009–2036.
32. *Aqueous System Modeling Course and Workshop. OLI Systems Inc*. New Jersey: Morris Plains, 2002.
33. Gurvich LV, Veyts IV, Alcock CB. *Thermodynamic Properties of Individual Substances*, 4th ed. Hemisphere Publishing Corporation, 1989.
34. Helgeson HC, Delany JM, Nesbitt HW, Bird DK. Summary and critique of the thermodynamic properties of rock-forming minerals. *Am J Sci*. 1978:1–229.
35. Chase MW, Davies CA, Downey JR, Frurip DJ, McDonald RA, Syverud AN. *JANAF Thermochemical Tables*, 3rd ed. J Phys and Chem Ref Data. 1985;14:1856.
36. Glushko VP, Medvedev VA, Bergman GA, Gurvich LV, Yungman VS, Alekseev VI, Kolesov VP, Vasil'ev BP, Reznitskii LA, Khodakovskii IL, Vorob'ev AF, Smirnova NL, Gal'chenko GL, Biryukov BP, Ioffe NT. *Thermal Constants of Compounds,* Part 1. USSR: Academy of Science, 1979;9:44.
37. Linke F. *Solubilities of Inorganic and Metal Organic Compounds*, 4th ed. Washington, DC: American Chemical Society, 1958;1:1487.
38. Sangwal K. Recent developments in understanding of the metastable zone width of different solute-solvent systems. *J Cryst Growth*. 2011;318:103–109.
39. Rafal M, Berthold JW, Scrivner NC, Grise SL. *Models for electrolyte solutions. Models for Thermodynamic and Phase Equilibria Calculations*. New York: Marcel Dekker, 1994:112–125.
40. Bromley LA,Thermodynamic properties of strong electrolytes in aqueous solutions. *AIChE J*. 1973;19:313–320.
41. Zemaitis JF. Predicting vapor-liquid equilibria in multicomponent aqueous solutions of electrolytes. In: Newman SA, Barner HE, Klein M, editors. *Thermodynamics of Aqueous Systems with Industrial Applications. ACS Symposium Series 133*; Washington, DC: American Chemical Society, 1980:227–246.
42. Seneviratne DS, Papangelakis VG, Zhou XY, Lvov SN. Potentiometric pH measurements in acidic sulfate solutions at 250°C relevant to pressure leaching. *Hydrometallurgy*. 2003;68: 131–139.
43. Casas JM, Papangelakis VG, Liu HX. Performance of three chemical models on the high-temperature aqueous $Al_2(SO_4)_3$-$MgSO_4$-H_2SO_4-H_2O system. *Ind Eng Chem Res*. 2005,44:2931–2941.
44. Moldoveanu GA, Papangelakis VG. Recovery of rare earth elements adsorbed on clay minerals: I. Desorption mechanism. *Hydrometallurgy*. 2012;117–118:71–78.
45. Ma JY, Li ZB. Chemical equilibrium modeling and experimental measurement of solubility for Friedel's salt in the Na-OH-Cl-NO_3-H_2O systems up to 200°C. *Ind Eng Chem Res*. 2010;49:8949–8958.
46. Ma JY, Li ZB, Xiao QG. A new process for Al_2O_3 production from low grade diasporic bauxite based on reactive silica dissolution and stabilization in NaOH-$NaAl(OH)_4$ media. *AIChE J*. 2012;58:2180–2191.
47. Lide DR. *CRC Handbook of Chemistry and Physics*, 89th ed. Boca Raton: CRC Press, 2009.
48. Li SW, Xu JH, Wang YJ, Luo GS. Liquid-liquid two-phase flow in pore array microstructured devices for scaling-up of nanoparticle preparation. *AIChE J*. 2009;55:3041–3051.
49. Rabesiaka M, Sghaier M, Fraisse B, Porte C, Havet J-L, Dichi E. Preparation of glycine polymorphs crystallized in water and physicochemical characterizations. *J Cryst Growth*. 2010;312:1860–1865.
50. Shiono T, Shiono,K, Miyamoto,K, Pezzotti G. Synthesis and characterization of $MgAl_2O_4$ spinel precursor from a heterogeneous alkoxide solution containing fine MgO powder. *J Am Ceram Soc*. 2000;83:235–237.
51. Carter RE. Mechanism of solid state reaction between MgO-Al_2O_3 and MgO-Fe_2O_3. *J Am Ceram Soc*. 1965;44:116–120.
52. Bakker WT, Lindasy JG. Reactive magnesia, preparation and properties. *Am Ceram Soc Bull*. 1994;41:1094–1097.
53. ISO 10081-1. *Basic Refractory Products—Classification—Part 1: Products Containing Less than 7% Carbon*. International Standards Organization. Committee TC-33 on Refractories, 1991.

Manuscript received May 30, 2012, and revision received Sept. 28, 2012.